Global sensitivity analysis of GEOS-Chem modeled ozone and hydrogen oxides during the INTEX campaigns

Kenneth E. Christian[1], William H. Brune[1], Jingqiu Mao[2], and Xinrong Ren[3,4]

[1]Department of Meteorology and Atmospheric Science, Pennsylvania State University, University Park, PA (USA)
[2]Department of Chemistry and Biochemistry and Geophysical Institute, University of Alaska at Fairbanks, Fairbanks, AK (USA)
[3]Department of Atmospheric and Oceanic Science, University of Maryland, College Park, MD (USA)
[4]Air Resources Laboratory, National Oceanic and Atmospheric Administration, College Park, MD (USA)

Correspondence to: Kenneth Christian (kec5366@psu.edu)

Abstract. Making sense of modeled atmospheric composition requires not only comparison to in situ measurements, but also knowing and quantifying the sensitivity of the model to its input factors. Using a global sensitivity method involving the simultaneous perturbation of many chemical transport model input factors, we find the model uncertainty for ozone (O_3), hydroxyl radical (OH), and hydroperoxyl radical (HO_2) mixing ratios and apportion this uncertainty to specific model inputs for the DC-8 flight tracks corresponding to the NASA INTEX campaigns of 2004 and 2006. In general, when uncertainties in modeled and measured quantities are accounted for, we find agreement between modeled and measured oxidant mixing ratios with the exception of ozone during the Houston flights of the INTEX-B campaign and HO_2 for the flights over the northernmost Pacific Ocean during INTEX-B. For ozone and OH, modeled mixing ratios were most sensitive to a bevy of emissions, notably lightning NO_x, various surface NO_x sources, and isoprene. HO_2 mixing ratios were most sensitive to CO and isoprene emissions as well as the aerosol uptake of HO_2. With ozone and OH being generally over predicted by the model, we find better agreement between modeled and measured vertical profiles when reducing NO_x emissions from surface as well as lightning sources.

1 Introduction

Air quality and atmospheric composition for the United States and North American continent is at an intersection between competing drivers. On one hand, emissions controls and cleaner burning fuel sources have resulted in a significant decrease in US NO_x ($NO_x \equiv NO + NO_2$) emissions (e.g., de Gouw et al., 2014). On the other, for many locations, especially in the western US, air quality has not improved proportionally to these emissions reductions, in part due to transport from Asia (Verstraeten et al., 2015; Lin et al., 2017). Clearly, a better understanding of the complicated processes governing atmospheric composition for North America will be vital in making informed regulatory decisions.

Correctly modeling atmospheric composition is a difficult endeavor, but one of great importance. Oxidants are of particular interest and importance when it comes to tropospheric chemical modeling and applications relating to both health and climate change including ozone, which has deleterious environmental and human health effects, and the hydroxyl radical (OH), which

largely determines the lifetimes of volatile organic compounds (VOCs) and species like carbon monoxide and methane. Thus, in trying to understand current and future air chemical processes, oxidants are a worthy place to start.

Modeling the composition of the atmosphere is complicated, notwithstanding the fact that model inputs, such as emissions, chemical reactions, and transport are not perfectly understood and cannot be perfectly represented in computer models. To make sense of these shortcomings, sensitivity and uncertainty analyses are useful tools in both determining the robustness of modeled results and identifying and quantifying sources of error. Generally, sensitivity analyses fall into two main camps: local and global. Local sensitivity analyses involve the perturbation of individual model inputs one at a time over a prescribed segment of the input space. Global sensitivity analyses, however, feature the simultaneous perturbation of multiple inputs across the breadth of their uncertainty ranges (Rabitz and Aliş, 1999; Saltelli et al., 2008). The advantage of these simultaneous perturbations is that non-linear interactions between model factors are allowed to propagate in global sensitivity analysis, an important advantage considering the nonlinear nature of the interactions between emissions, chemistry, and meteorology that underlie atmospheric composition modeling.

With the computationally expensive nature of running chemical transport models (CTMs) such as the GEOS-Chem (Goddard Earth Observing System-Chemistry) model used in this study, global sensitivity methods, which require hundreds of model runs to provide meaningful statistical results, have been unsurprisingly lacking from the literature save for some recent work (Brewer et al., 2017; Christian et al., 2017). Instead, the sensitivity analyses of GEOS-Chem modeled results has either used local methods in which the factor of interest is perturbed individually and compared to the model state without this perturbation or the GEOS-Chem adjoint (Henze et al., 2007). These local and adjoint tests have been completed for a variety of emissions (e.g., Fiore et al., 2002; Guerova et al., 2006; Jaeglé et al., 2005; Fiore et al., 2005; Mao et al., 2013b; Xu et al., 2013; Qu et al., 2017), meteorological (Wu et al., 2007; Heald et al., 2010), and chemical factors (Mao et al., 2013a; Newsome and Evans, 2017). While adjoint methods have improved our understanding of atmospheric processes and helped in ascertaining various emissions, there are some drawbacks when compared to global sensitivity methods. For one, without perturbing factors across the entirety of their uncertainty ranges, adjoint sensitivity analyses do not provide a complete picture of model uncertainty. Additionally, adjoint sensitivity methods can only provide model sensitivities for one model output or cost function at a time. With global sensitivity analyses, we can calculate model sensitivities for a variety of different model outputs and domains for negligible additional computational cost. The drawback for this flexibility in global sensitivity analyses is the high computational cost of creating hundreds of chemical transport model runs. Considering the popularity of adjoint and other sensitivity analysis methods, we see value in exploring this different and complementary method.

To gain a better grasp of air chemical processes over North America, and the regions both up and downwind of the continent, various academic and governmental entities took part in the NASA sponsored Intercontinental Transport Experiment (INTEX) campaigns, part of the International Consortium on Atmospheric Transport and Transformation (ICARTT). The INTEX-NA (INTEX-North America) part of the ICARTT campaign took place in two phases: INTEX-A (summer 2004) and INTEX-B (spring 2006). The INTEX-A campaign sought to characterize the air chemistry of eastern and central United States and Canada and was based out of Pease Air National Guard Base in Portsmouth, New Hampshire and Mid America Airport/Scott Air Force Base in Western Illinois (St. Louis, Missouri metropolitan area). After INTEX-A, which characterized the air composition of

the continent, INTEX-B sought to study both the North Pacific background and Asian outflow, and Mexican outflow over the Gulf of Mexico. These flights were based out of Houston, Texas; Honolulu, Hawaii; and Anchorage, Alaska.

Through a global sensitivity analysis of modeled oxidants during INTEX we aim to meet a few goals. One, determine the uncertainty in modeled results arising from uncertainty in the model inputs. Two, determine which of these inputs are most responsible for the uncertainty in the modeled results. Three, determine which perturbations to the model allow for a better match to in situ observations collected during the campaigns. In allowing for the calculation of model uncertainties and sensitivities to many input factors, a global sensitivity analysis is well suited for these objectives. Knowing the model sensitivities will provide direction not only for future model improvements but also for identifying the most impactful directions for future research.

2   Methods

In the following section, we briefly describe the methods employed in this study. For a more detailed description, please refer to Christian et al. (2017).

2.1   Model

We use in this study the default GEOS-Chem model (v9-02), a widely-used global chemical transport model (Bey et al., 2001). There are a few different resolutions available to modelers, but to facilitate the construction of our sensitivity ensemble, we used the coarser horizontal resolution of $4° \times 5°$. Model resolution is an important consideration for chemical transport models, but the errors associated with resolution choices are usually less than those coming from chemistry, meteorology, and emissions (Wild and Prather, 2006). In general, there were typically small differences between modeled results using either $4° \times 5°$ or $2° \times 2.5°$ resolutions (Figs. S1, S2, S3, and S4) but we illustrate in our results where this is not the case.

Our GEOS-Chem model runs were driven by the Modern-Era Retrospective Analysis for Research (MERRA) meteorological model for INTEX-A, while the INTEX-B model runs were driven by GEOS-5 (Goddard Earth Observing System). This difference is due to GEOS-5 model availability not extending far enough back in time to facilitate its inclusion in the INTEX-A runs. When comparing modeled results for INTEX-B running MERRA, there were extremely small differences between the modeled results using either meteorological model. As uncertainties are not published for the meteorological models, we define our meteorological uncertainties as the average of the monthly standard deviations of the difference between GEOS-4 and GEOS-5 meteorological fields for 2005, a year of overlap between the models.

Generally, the model ensemble made use of the default emissions inventories. For many industrialized regions, including much of North America, Europe, and East Asia, the regional emissions inventories overwrote the default Emission Database for Global Atmospheric Research (EDGAR) or REanalysis of the TROpospheric chemical composition (RETRO) fields. Lightning NO_x is treated through the scheme of Price and Rind (1992) with close to a factor of 2 greater lightning NO_x yield over the midlatitudes compared to the tropics (500 mol flash^{-1} vs 260 mol flash^{-1}). The differential between the treatment of tropical and midlatitudinal NO_x yields was created to match observations (Huntrieser et al., 2007, 2008; Hudman et al., 2007). Recent

research has questioned the arbitrary geographic boundary in lightning NO_x yields and show the sensitivity of regions around the tropical/midlatitude boundary to this treatment (Zhang et al., 2014; Travis et al., 2016). We show in our results where this is a consideration. Transport of stratospheric ozone into the troposphere is parameterized by the Synoz algorithm (McLinden et al., 2000) in which 500 $TGyr^{-1}$ of ozone is advected through the tropopause.

5   Uncertainties in emissions in this study ranged from factors of 2 to 3 with higher uncertainties in biomass and soils emissions. This higher uncertainty is due to the wide range of values in the literature, (e.g., Jaeglé et al., 2005; Schumann and Huntrieser, 2007; Vinken et al., 2014). While some of the uncertainties in these emissions are correlated in reality, we treat all the emitted species within these emissions inventories individually in this analysis. This treatment allows for the pinpointing of the individual species or processes resulting in model uncertainty. We assume uncertainties of a factor of 2 for lightning

10 NO_x (Liaskos et al., 2015), biogenic VOC (Guenther et al., 2012), stratospheric-tropospheric exchange of ozone, default and regional anthropogenic, ship, and methyl bromoform emissions.

    Chemical rate uncertainties came from NASA's Jet Propulsion Laboratory's (JPL's) evaluation (Sander et al., 2011). For the most part, chemical rate uncertainties are lower than those of emissions inventories, around 20-30% for many chemical kinetic and photolysis rates. Uncertainty in the rate of aerosol particle uptake of the hydroperoxyl radical (HO_2) (gamma HO_2) was

15 assumed to be a factor of 3. In the case of gamma HO_2, we use the default model treatment in which $\gamma_{HO_2} = 0.2$ (Jacob, 2000) and yields H_2O, a terminal HO_x ($HO_x \equiv OH + HO_2$) reaction (Mao et al., 2013a). Not only is there uncertainty in the rate of this uptake, but there is also uncertainty in the product of this reaction, and whether or not H_2O_2 is produced instead of or alongside H_2O. In this study, we generally find small differences between these possibilities.

2.2   Global Sensitivity Analysis

20 The Random Sampling-High Dimensional Model Representation (RS-HDMR) (Rabitz and Aliş, 1999; Li et al., 2001) is a global sensitivity analysis method used in conjunction with other air chemistry studies (Chen and Brune, 2012; Chen et al., 2012; Christian et al., 2017). The method involves the simultaneous perturbation of model factors across their respective uncertainties. Instead of randomly sampling the input space as prescribed, we sample using a quasi-random number sequence (Sobol, 1976). Quasi-random sampling allows for a more efficient sampling of the input space facilitating reliable results with

25 fewer runs. Following common practice, we discarded a set of initial values when creating the quasi-random sequence, in our case the first 512, as a spin up.

    Previous sensitivity analyses implementing the HDMR method or its variations often use thousands of model runs. With CTMs like GEOS-Chem, this computational cost is prohibitive. Instead, we limit our ensemble to 512 model runs. As seen in Lu et al. (2013) and this study, we find the sensitivity results to converge after a few hundred runs supplying confidence in the

30 indices calculated here.

    Conceptually, the HDMR method describes the modeled output as a collection of polynomials relating the model output to the inputs, both individually and collectively.

$$f(x) = f_0 + \sum_{i=1}^{n} f_i(x_i) + \sum_{1 \le i \le n} f_{ij}(x_i, x_j) + ... + f_{12...n}(x_1, ..., x_n) \tag{1}$$

Here f_0 is the zeroth order component, a constant equivalent to the mean (Eq. (2)) (where s represents the model run and N represents the total number of model runs), $f_i(x_i)$ is the first order effect corresponding to the independent effect of the input x_i on the output (Eq. (3)) (where i = 1, 2, ..., n where n is the number of factors included in the analysis), f_{ij} corresponding to the second order effect on the output of inputs x_i and x_j working cooperatively to influence the output (where i = 1, 2, ..., n; j = 1, 2, ..., n; and $i \neq j$), on down to the nth order effect on the output by all the inputs working cooperatively (Rabitz and Aliş, 1999).

$$f_0 \approx \frac{1}{N} \sum_{s=1}^{N} f(x^s) \tag{2}$$

$$f_i(x_i) \approx \sum_{r=1}^{k_i} \alpha_r^i \varphi_r(x_i) \tag{3}$$

Here φ represents orthonormal polynomials, k_i represents the orders of the polynomials fitted for each input, and α is the constant coefficient for each polynomial. Similarly to Eq. (3), polynomials created to represent second and higher order effects such as $f_{ij}(x_i, x_j)$ are created using orthonormal polynomials and constant coefficients. For a more detailed description of the calculation of the orthonormal basis polynomials (φ) and the constant coefficients (α), refer to (Li et al., 2002, 2003).

With each component function being orthogonal, the total variance can be split into a summation of the variances of all the polynomials in Eq. (3) (e.g., Li et al., 2010). For example:

$$V(f(x)) = \sum_{i=1}^{n} V(f_i(x_i)) + \sum_{1 \leq i \leq n} V(f_{ij}(x_i, x_j)) + ... + V(f_{12...n}(x_1, ..., x_n)) \tag{4}$$

Where $V(f_i(x_i))$ represents the variance of the first order effect due to the input x_i and so forth. Normalizing the individual variances in Eq. (4) by the total variance results in the creation of sensitivity indices for each input (Eq. (5)). While sensitivity indices can similarly be found for the functions relating to the second and higher order interactions between inputs, these indices need more model runs than presented here for meaningful results. The end result of the sensitivity index calculations are a series of sensitivity indices representing the portion of the output variance attributable to each input factor with the residual portion attributable to second and higher order factor-factor interactions (Eq. (6)).

$$S_i = \frac{V(f_i(x_i))}{V(f(x)))} \tag{5}$$

$$1 = \sum_{i=1}^{n} S_i + \text{higher order sensitivities} \tag{6}$$

To focus the RS-HDMR analysis on the most important model inputs, we completed a preliminary Morris method sensitivity test (Morris, 1991) for both the INTEX-A and INTEX-B domains, including any factor within around 15 % of the most sensitive factor for ozone, OH, or HO_2. Using the Morris Method as a preliminary step in RS-HDMR tests is a common practice in multiple RS-HDMR sensitivity studies (Ziehn et al., 2009; Chen et al., 2012; Lu et al., 2013). This prescreening process resulted in 39 factors being included in the RS-HDMR analysis for INTEX-A and 47 for INTEX-B (Tables 1 and 2 respectively).

2.2.1 Uncertainties

Before perturbing the inputs and running the model, the next step was to create the uncertainty distributions for the prescreened model inputs using the uncertainties listed earlier in the methods section and in Tables 1 and 2. For the majority of the factors, we used lognormal uncertainty distributions where the standard deviations were determined by σ = (f-1/f)/2 (Gao et al., 1995; Yang et al., 1995) where f is the published uncertainty factor. Normal distributions were used for some meteorological factors (relative and specific humidity, soil wetness, and temperature). To allow model perturbations time to spread globally, all runs in the model ensemble were spun up 9 months before the first flight for the respective campaigns.

2.2.2 Calculation of sensitivity indices

RS-HDMR sensitivity indices were calculated using graphical user interface - HDMR (GUI-HDMR), a free MATLAB package (http://www.gui-hdmr.de) (Ziehn and Tomlin, 2009). As in Christian et al. (2017), in running GUI-HDMR, the inputs were scaled according to their percentiles within their respective uncertainty distributions and the correlation method option was applied (Kalos and Whitlock, 1986; Li et al., 2003).

2.3 Measurements

The NASA DC-8 carried a suite of state of the science instruments during both INTEX-A and INTEX-B (Singh et al., 2006, 2009). For comparison to the modeled HO_x mixing ratios, we compare to the measurements taken by Pennsylvania State University's Airborne Tropospheric Hydrogen Oxides Sensor (ATHOS) (Brune et al., 1998). In this instrument, HO_x is measured using laser-induced fluorescence (LIF). Ozone mixing ratios were measured by NASA-LaRC (Langley Research Center) using nitric oxide chemiluminescence (Weinheimer et al., 1994).

Interferences in OH and HO_2 measurements are a concern with ATHOS and other measurement techniques (Ren et al., 2004; Fuchs et al., 2011; Mao et al., 2012). Typically these interferences are less than a factor of 2 for HO_2 and between a factor of 1.2 and 3 for OH. Interferences in OH and HO_2 are mostly a concern in the boundary layer above forested or urban environments as they occur in the presence of alkenes or aromatics. For much of the mid to upper troposphere and the marine domains sampled in much of INTEX-B, these interferences will be negligible.

2.4 Box Model

In contrast to our previous study, we also analyze oxidant mixing ratios calculated by a time dependent zero dimensional box model providing an additional comparison to both the chemical transport model and the measurements. In this modeling approach, HO_x mixing ratios are calculated using a model constrained by other trace gas measurements measured aboard the DC-8 and is integrated until the box model reaches a consistent diurnal steady state. At a minimum, the model is constrained by ozone, CO, NO_2, non-methane hydrocarbons, acetone, methanol, temperature, dew and frost point of water, pressure, and calculated photolysis frequencies (Ren et al., 2008). These model calculations are available alongside the measurements in the

NASA Langley archives for the campaigns. For a more detailed description of the box model, please refer to Crawford et al. (1999); Olson et al. (2004); Ren et al. (2008).

2.5 Comparison of modeled and measured results

Allowing for the comparison of the model ensemble to the aircraft observations, modeled results were output in one-minute
5 intervals along the DC-8 flight track using the Planeflight option within GEOS-Chem. With a relatively coarse horizontal resolution chosen, it is a concern that GEOS-Chem would miss meso to synoptic scale features that could be important for correctly modeling oxidant abundances. With our analysis averaging over many flights, many of these differences would be averaged out.

3 Results

10 During INTEX-A, the NASA DC-8 primarily sampled the eastern half of the United States and Canada during the summer of 2004. In contrast to the mostly continental study area of INTEX-A, INTEX-B largely took place over the Gulf of Mexico and the North Pacific (Fig. 1) in the spring of 2006. In both campaigns, the aircraft sampled the troposphere at a variety of altitudes from the surface to near the tropopause (bar graphs in Figs. 2, 3, 4, and 5). In INTEX-B, the results are split into three separate domains outlined in Fig. 1 and named according to the city in which the flights were based: Houston, Texas; Honolulu, Hawaii;
15 and Anchorage, Alaska.

3.1 Uncertainty

3.1.1 INTEX-A

For ozone and OH, GEOS-Chem modeled mixing ratios were consistently higher than measurements (Fig. 2). Throughout the vertical column, GEOS-Chem modeled ozone was around 10 ppb greater than measurements. For OH, modeled and measured
20 values were similar close to the surface, but the disagreement widens higher, with modeled values being a factor of $\sim$1.6 greater than measurements around 6 km. Unlike GEOS-Chem, the box model generally agreed with the measured OH profiles suggesting that the model errors for OH are likely arising outside of the chemical mechanism, such as emissions sources. In contrast to ozone and OH, measured HO_2 profiles were generally greater than the model ensemble with the widest disagreement coming close to the surface. Unlike OH, HO_2 profiles modeled by the box model generally agreed with GEOS-Chem more
25 than they did the measurements. This model-model agreement suggests that either the model errors may be arising from the largely similar chemistry of the two models or the measurements are incorrect, perhaps due to peroxy radical interference. The agreement between GEOS-Chem and ATHOS HO_x profiles presented here is different than Hudman et al. (2007) due to errors found in the calibration of the measurements (Ren et al., 2008). At all altitudes there were small differences between the finer $2°$ x $2.5°$ and the coarser $4°$ x $5°$ ensemble. Specifically these differences were less than 4 ppb for ozone, a few hundredths of
30 a ppt for OH, and less than 1 ppt for HO_2.

Part of this disagreement in mixing ratios could be attributed to uncertainties in the modeled values. We find 1σ uncertainties for the modeled oxidant mixing ratios to range from 19-23 % for ozone, 27-36 % for OH, and 18-37 % for HO_2 in the different vertical bins. When taking into account both uncertainties in model input factors and measurements, we find there to be overlap between all the oxidant profiles. This overlap shows that the uncertainties in the model and measurements can explain
5   the difference between the model and measured profiles.

3.1.2   INTEX-B Houston

The vertical profiles for ozone, OH, and HO_2 all follow a similar pattern: general agreement between measured and modeled mixing ratios near the surface turning to model overestimation above 4 km or so (Fig. 3). In the case of ozone, the model-measurement gap persists even when accounting for measurement uncertainty, especially from 5 km higher. As a consequence
10   of this model overprediction of ozone, OH and HO_2 both are also overpredicted by GEOS-Chem above 4-5 km, but unlike ozone there is overlap at all levels between the measured and modeled values when uncertainties in both are taken into account. Generally, there are small differences between the median of the $4° \times 5°$ model ensemble and a finer resolution $2° \times 2.5°$ run, however, there are some larger differences between these two possibilities, with ozone mixing ratios being reduced by 7-9 ppb above 5 km in the finer resolution. Conversely, below 5 km, the finer resolution run produces higher OH mixing ratios (about
15   0.06 ppt or $\sim$30 % higher), roughly on the order of the 1σ model uncertainty. Differences between HO_2 profiles using either model resolution were within a few ppt at all altitudes and within 1 ppt in most of the vertical bins.

Unlike GEOS-Chem, the box model tended to better agree with measurements higher in the troposphere for OH (Fig. 3). In the case of OH mixing ratios, the box model was around a factor of 2 greater than measurements in the first vertical bin and around 30 % greater up through 4 km. Higher than 4 km, the box model and measurements largely agreed. For HO_2 mixing
20   ratios, the box model was greater than observations at all heights but was marginally closer than GEOS-Chem to the measured profile.

Model ozone uncertainty was largely altitude independent, running between 19 and 21 % below 8 km. Uncertainty in modeled OH was between 28 and 40 % with uncertainty on a percentage basis ranging highest near the surface and above 7 km (Fig. 3). Model HO_2 uncertainty followed a similar vertical pattern to OH with the highest uncertainty coming near the surface
25   ($\sim$30 %) and lower in the middle troposphere (18-20 % from 3 km up through 8 km).

3.1.3   INTEX-B Honolulu

Vertically, uncertainty in ozone is nearly altitude independent, ranging between 17.5 and 20.5 % (1σ) (Fig. 4). While GEOS-Chem on average comes close to the average measured values, the model fails in matching the measured profile shape. Near the surface, the GEOS-Chem is around 12 ppb less than measured values. This underprediction shifts to overprediction around
30   4 km with the model overpredicting 25-30 ppb around 9-10 km. This under and overprediction by the model at low and high altitudes is outside the model and measurement uncertainties. Differences between the finer $2° \times 2.5°$ and the coarser $4° \times 5°$ ensemble were smaller than these model-measurement disagreements. At nearly every altitude the ozone mixing ratios were within 10 ppb with no consistent positive or negative bias.

In contrast to ozone, the uncertainty in OH mixing ratios is high and vertically variable (Fig. 4). From 0-3 km, uncertainty is roughly around 32-36 % before increasing through the middle troposphere to 38-40 %. For all altitudes, measured and model values were within each other's uncertainty range. The box model agreed well with OH measured mixing ratios, especially above 5 km with more modest agreement and slight overprediction below. Between the finer 2° x 2.5° and the coarser 4° x 5°
5   ensemble we found generally higher OH mixing ratios, but within a few hundredths of a ppt.

Compared to OH, uncertainty in HO_2 mixing ratios is lower but follows the same pattern of increasing with altitude (Fig. 4). We find uncertainty rising from 16-20 % between the surface and 4 km, to between 23-30 % from 5 km higher. Generally, GEOS-Chem replicated the measured HO_2 mixing ratio profile within a couple ppt. Differences between the finer and coarser resolution choices resulted in differences around or less than 2 ppt below 9 km. Like OH, the box model generally agreed well
10 with measured HO_2 mixing ratios. The overall agreement between the oxidant profiles in this domain may be attributable to the reduced surface emissions sources in this remote, Central Pacific domain.

3.1.4   INTEX-B Anchorage

In contrast to the previous regions analyzed here, measured ozone, OH, and HO_2 mixing ratios were generally greater than GEOS-Chem modeled values in nearly every vertical bin (Fig. 5). Ozone mixing ratios were underpredicted by the model
15 around 10 ppb, with the difference between modeled and measured values maxing out at 17 ppb around 4 km. Except for near the surface where the model was around 0.04 ppt too high and above 8 km, GEOS-Chem generally underrepresented OH by a couple hundredths of a ppt. These differences are within the model and measurement uncertainty. HO_2 mixing ratios showed some of the widest disagreement between modeled and measured values with the model being anywhere from a 1.6 ppt short near the surface to upwards of 6.8 ppt between 3 and 4 km. In this domain, we found small differences in oxidant mixing ratios
20 between the finer 2° x 2.5° and the coarser 4° x 5° ensemble. Specifically, modeled ozone was around 0-4 ppb higher in the fine resolution case, OH 1-3 hundredths of a ppt higher in the fine resolution case, and HO_2 mixing ratios within a few tenths of a ppt.

Compared to GEOS-Chem, the box model performs better in matching the measured OH and HO_2 mixing ratio profiles. In particular, while still somewhat underpredicting HO_2 mixing ratios, the box model does match the shape of the measured HO_2
25 profile unlike GEOS-Chem (Fig. 5). Because of this relatively close match between the box model and the measurements, the disagreement between GEOS-Chem and the measurements could be arising outside of the chemical kinetics. Conversely, the box model may be better matching the measured profile just due to its lack of aerosol uptake of HO_2. In the Arctic, the aerosol uptake of HO_2 is a major loss pathway for HO_2 (Whalley et al., 2015). Without this loss pathway, the box model may have artificially high HO_2 mixing ratios.
30 Uncertainty in modeled ozone mixing ratios was relatively low, ranging between 13 and 20 %. In contrast, uncertainties in both OH and HO_2 mixing ratios were considerable ranging between 34 and 57 % for OH and 21 and 40 % for HO_2 (Fig. 5). This higher uncertainty is in part a product of the very low mixing ratios modeled in this northern domain with OH mixing ratios being less than a tenth of a ppt for most of the vertical column and modeled HO_2 mixing ratios in a range between 6 and 9 ppt.

3.1.5 Takeaways from uncertainties

Despite the geographic range of the regions presented here, there are many similarities to highlight. For instance, uncertainties in GEOS-Chem modeled mixing ratios for ozone, OH, and HO_2 were largely similar. As a rule of thumb, uncertainties in ozone mixing ratios were around 20 %, OH between 25 and 40 %, and HO_2 between 20 and 35 %. Also, for most regions, when uncertainties in both GEOS-Chem and measurements are taken into account, there is general agreement between oxidant mixing ratios with the exception of ozone profiles in the higher altitude Houston based INTEX-B flights and ozone in a few other vertical bins in the Pacific INTEX-B flights.

3.2 Sensitivities

To explore from where the model-measurement disagreements may be coming, Figs. 6, 7, 8, and 9 show the median first order sensitivity indices across INTEX-A and regional INTEX-B flights for ozone, OH, and HO_2. As the sensitivities of ozone, OH and HO_2 varied with altitude, we show the analysis for the 0-1 km, 3-4 km, and 7-8 km vertical bins. The "missing" portion of the pies represents the portion of the model variance not explained by uncertainties in individual factors, rather factor-factor interactions.

3.2.1 INTEX-A

Generally ozone was most sensitive to emissions, particularly NO_x and isoprene (Fig. 6). Near the surface, ozone was most sensitive to the EPA-NEI (Environmental Protection Agency–National Emissions Inventory) NO_x emissions and isoprene (S_i = 0.21 and 0.20 respectively). A few kilometers up, this sensitivity to surface NO_x emissions is replaced by sensitivity to lightning NO_x (S_i = 0.28 and 0.30 for 3-4 km and 7-8 km respectively). Sensitivity to chemical factors such as the NO_2 + OH reaction rate, and the NO_2 photolysis rate were largely altitude independent (S_i between 0.08 and 0.13 for k[NO_2 + OH]; S_i = 0.07-0.08 for j[NO_2]).

Sensitivities for OH largely mirrored those of ozone (Fig. 6). As photolysis of ozone in the presence of water vapor leads directly to the production of OH, this is unsurprising. In addition to NO_x and isoprene emissions mentioned with ozone, we also find OH above 3 km to be sensitive to CO emissions, especially from biomass burning (S_i = 0.16 between 3-4 km and S_i = 0.10 between 7-8km).

Near the surface where modeled aerosol concentrations are greatest, HO_2 is most sensitive to the aerosol uptake of HO_2 and isoprene emissions (S_i = 0.28 and 0.25 respectively) (Fig. 2). This sensitivity to aerosol uptake is reduced higher in the troposphere with biomass CO (S_i = 0.26 at 3-4 km and S_i = 0.18 between 7-8 km), lightning NO_x (S_i = 0.12 at 7-8 km), and isoprene emissions (S_i= 0.15 between 3 and 4 km and S_i = 0.26 between 7 and 8 km) being the dominant sources of the uncertainty above 3 km. As uncertainty in gamma HO_2 is not limited to just the rate of the reaction, but also to the product, we examined the modeled profiles in a model run having gamma HO_2 producing H_2O_2 rather than H_2O. With small differences generally around or less than half a ppt for HO_2 and likewise small differences for OH and ozone, HO_2 and the other oxidants are rather insensitive to this difference. Sensitivity to isoprene emissions is roughly altitude independent. As

isoprene's lifetime is shorter than the timescales to allow consequential transport past the boundary layer, the sensitivity of HO_2 to isoprene emissions in the mid to free troposphere is almost certainly due to chemistry relating to secondary and higher order isoprene products such as the photolysis of formaldehyde and acetaldehyde.

3.2.2 INTEX-B Houston

5   As with INTEX-A, ozone is largely sensitive to NO_x emission inventories, specifically soil NO_x near the surface and lightning NO_x from 3 km higher (Fig. 7). In contrast to the height dependencies in the emissions inventories sensitivities, sensitivity to chemical factors were generally altitude independent with sensitivities to k[NO_2 + OH] ranging between S_i values of 0.07 and 0.09 and j[NO_2] and j[O_3] between 0.03 and 0.08. For emission factors, in the lowest 1 km apart from soil NO_x emissions (S_i = 0.28), we also find isoprene emissions (S_i = 0.08), and EDGAR NO_x emissions (S_i = 0.07) having S_i values greater than

10   0.05. From 3-4 km higher, lightning NO_x becomes the dominant source of uncertainty with S_i values of 0.30 around 4 km and higher between 7 and 8 km (S_i = 0.41). In these higher altitude bins, we also find ozone to have greater sensitivity to biomass CO emissions with S_i values of 0.07 between 3 and 4 km and S_i = 0.09 between 7 and 8 km.

   Similar to ozone, while we find OH to be most sensitive to emissions sources, the sensitivity to these sources are altitude dependent (Fig. 7). Near the surface, OH is most sensitive to isoprene and soil NO_x emissions sources (S_i values of 0.21 and

15   0.15 respectively). Chemical factors such as k[NO_2 + OH], aerosol uptake of HO_2, and j[NO_2] also had S_i values greater than 0.05 (0.09, 0.08, and 0.07 respectively). Higher, lightning NO_x becomes the dominant source of uncertainty for OH mixing ratios with S_i values of 0.21 in the 3-4 km bin and 0.54 for the 7-8 km bin.

   For HO_2 mixing ratios, near the surface we find gamma HO_2 to be responsible for about half of the model uncertainty (S_i = 0.51) with isoprene emissions being the only other factor with S_i > 0.05 (S_i = 0.16) (Fig. 7). This dominance by gamma HO_2,

20   though, is restricted to near the surface where aerosol concentrations are highest. In fact, higher than 3 km, we find biomass CO emissions to become the dominant source of uncertainty (S_i = 0.27 for 3-4 km, S_i = 0.38 for 7-8 km). Sensitivity to isoprene emissions is similar between 3-4 km and 7-8 km with S_i values of 0.13 and 0.14 respectively.

3.2.3 INTEX-B Honolulu

   For the flights based out of Honolulu, near surface ozone was most sensitive to surface emissions sources in the first vertical

25   kilometer with ship NO_x (S_i = 0.27) and methyl bromoform emissions (S_i = 0.07) and a variety of chemical factors such as the ozone photolysis rate (j[O_3] (S_i = 0.14), k[NO_2+oh] (S_i = 0.06), j[HOBr] (S_i = 0.05), j[NO_2] (S_i = 0.05)) (Fig. 8). Higher, ozone becomes sensitive to other emissions sources, especially lightning NO_x (S_i = 0.11 and 0.25 at 3-4 km and 7-8 km respectively), and to a lesser extent, soil, and E. Asian NO_x and isoprene emissions. These latter emissions sources are noteworthy as they illustrate the sensitivity of this region to non-local upwind emission sources as there are not any appreciable isoprene or soil

30   NO_x emissions over the remote north central Pacific. In addition to emissions sources, ozone also showed moderate sensitivity to chemical factors. In particular, the photolysis rate of ozone, in spite of its low uncertainty (20 %), had sensitivity indices ranging between 0.10 and 0.15 between the surface and 5 km. The NO_2 + OH reaction rate also had sensitivity indices about 0.07 at most altitudes.

OH mixing ratios were largely sensitive to the same factors as ozone (Fig. 8). Near the surface OH was largely sensitive to ship NO_x emissions (S_i = 0.38), both biomass and E. Asia CO, $j[O_3]$, $k[NO_2 + OH]$, and $j[NO_2]$ (S_i = 0.09, 0.08, 0.08, 0.06, and 0.05 respectively). Above 3 km, there is not any one factor that overwhelmingly contributes to the uncertainty, but CO and NO_x emissions, along with the photolysis rate of ozone and the NO_2 + OH reaction rate all had S_i values around greater than 0.05 for the higher altitude bins.

Like the Houston flights, HO_2 mixing ratios were largely sensitive to CO emissions, NO_x emissions, and aerosol uptake of HO_2, only sensitivity to aerosol uptake is reversed vertically with higher sensitivities coming in the upper troposphere rather than near the surface (S_i = 0.10, 0.16, 0.30 for 0-1 km, 3-4 km, and 7-8 km vertical bins) (Fig. 8). This is a result of the modeled aerosol concentrations being highest near the surface for the Houston flights, and highest in the upper reaches of the troposphere for the Honolulu flights.

3.2.4 INTEX-B Anchorage

Near the surface, ozone sensitivity was dominated by ship NO_x emissions (S_i = 0.52), and to a much lesser extent photolysis of HOBr (S_i = 0.06). Higher, a host of emissions factors become more important with bromoform emissions (S_i = 0.11 for 3-4 km and S_i = 0.09 for 7-8 km), soil NO_x (S_i = 0.10 and 0.11 for 3-4 km and 7-8 km respectively), and lightning NO_x (S_i = 0.13 at 7-8 km) (Fig. 9). Chemical factors such as $k[NO_2 + OH]$ and $j[NO_2]$ also were responsible for between 6 and 8 % of the uncertainty for both the 3-4 km and 7-8 km altitude bins.

Like ozone, OH was overwhelmingly sensitive to ship NO_x emissions (S_i = 0.50) with this one factor being responsible for around half the model uncertainty (Fig. 9). At 3-4 km, this sensitivity to ship NO_x emissions is replaced by CO emissions from E. Asia and biomass burning and soil NO_x (S_i = 0.11 for E. Asia CO, S_i = 0.09 for biomass CO and soil NO_x). From 3 km higher, OH mixing ratios are most sensitive to the aerosol uptake of HO_2 (S_i = 0.14 at 3-4 km, S_i = 0.29 at 7-8 km).

At all but the highest altitudes, modeled HO_2 mixing ratios were overwhelmingly sensitive to the aerosol uptake of HO_2 (gamma HO_2) with this one factor contributing around half the model uncertainty (S_i = 0.49 at 0-1 km, S_i = 0.57 at both 3-4 km and 7-8 km) (Fig. 9). This dominance of gamma HO_2 on HO_2 mixing ratios has been noted before in the similar ARCTAS-A (Arctic Research of the Composition of the Troposphere from Aircraft and Satellites) domain (Christian et al., 2017).

3.3 Discussion of results

Broadly speaking, measured and GEOS-Chem modeled oxidant profiles agreed to some extent in most of the cases outlined here. However, with 512 model runs for each campaign representing various combinations of perturbations to the inputs, it raises the question: which ensemble members fit the measured profiles best? With 512 model runs with various perturbations of the inputs, some members did come much closer to matching the measured profiles. In the following subsections we describe the commonalities among these better performing ensemble members' perturbations to NO_x emissions and aerosol uptake.

3.3.1 NO$_x$ emissions

For all the regions presented here, GEOS-Chem modeled and measured ozone and OH profiles have closer agreement with lower lightning NO$_x$ emissions than emitted by default. In examining the closest 25 model ensemble members for each region and oxidant, we find reductions in their lightning NO$_x$ emissions anywhere from $\sim$25 % for Anchorage INTEX-B ozone and OH, INTEX-A ozone, Honolulu INTEX-B OH, to around a factor of 2 reduction for INTEX-A OH, Houston INTEX-B ozone and OH, and Honolulu INTEX-B ozone. Considering GEOS-Chem tended to overpredict ozone and OH, especially at higher altitudes, it is unsurprising there is better agreement with lower lightning NO$_x$ emissions.

The vertical profiles of NO and NO$_2$ (Fig. S5) somewhat corroborate this overestimate of NO$_x$ emissions in INTEX-A and can explain the overestimate of ozone. In INTEX-A, we found modeled NO$_2$ to be consistently greater than their respective measured values. Near the surface, this difference can be anywhere between 50 % and factor of 2 or greater for NO$_2$ with the greatest difference on an absolute basis near the surface (0-1 km) and on a percentage basis in the middle troposphere (between 5 and 7 km). In contrast to INTEX-A NO$_2$ mixing ratios, NO was underpredicted by the model with the exception of the first vertical kilometer. With high NO$_2$ and low NO, the model steady-state ozone concentrations would be elevated as ozone concentrations are generally proportional to the [NO$_2$]/[NO] ratio (e.g., Chameides and Walker, 1973). In the Houston based INTEX-B flights, we found NO$_2$ to have modeled mixing ratios greater than measured between the surface and 1 km and above 5 km (Fig. S6). Between 5 and 9 km, NO and NO$_2$ mixing ratios are between 10 and 25 ppt too high in the model compared to measurements.

This model NO$_x$ overestimate is similar to results found in Travis et al. (2016) for the SEAC^{4}RS campaign. In the case of Travis et al. (2016), GEOS-Chem more closely matched observations when the United States regional NO$_x$ emissions were reduced by a factor of 2. The blue lines in Figs. 10 and 11 illustrate the better model-measurement agreement, especially for ozone, when both EPA-NEI and lightning NO$_x$ emissions are reduced by a factor of 2 for INTEX-A and Houston based INTEX-B flights. In the case of lightning NO$_x$, this factor of 2 reduction is similar to the difference between modeled lightning NO$_x$ production in the tropics versus the midlatitudes (north of 23°N for North America).

In the case of the INTEX-A flights, this reduction in NO$_x$ emissions eliminates much of the model-measurement disagreement, especially for ozone, but unlike INTEX-A, the Houston based INTEX-B GEOS-Chem model-measurement disagreement is not fully bridged for ozone, especially in the upper troposphere. This persistent disagreement suggests that lightning NO$_x$ emissions are not solely to blame for the upper altitude disagreement in ozone mixing ratios for the Houston based INTEX-B flights.

In addition to lightning NO$_x$, the Pacific flights of INTEX-B were also sensitive to ship NO$_x$ emissions, especially for the near surface vertical bins. For ozone, the 25 best matching model ensemble members had higher ship NO$_x$ emissions (65 % greater for Honolulu and 25 % greater for Anchorage flights). Since ozone was underpredicted by the model in conjunction with NO$_x$ (Figs. S7 and S8), increasing NO$_x$ emissions would presumably ameliorate some of this model-measurement disagreement. While this strong sensitivity to shipping emissions was not found during the ARCTAS campaign, this difference is likely a result of the more southerly direction, and thus more maritime domain, of the INTEX-B flights out of Anchorage,

rather than the more continental flights of the ARCTAS campaign. Model treatment of ship emissions is unique in comparison to other anthropogenic sources. In order to approximate the complex and non-linear chemistry within ship exhaust plumes, NO_x emissions are modified and partitioned via the PARAmeterization of emitted NOX (PARANOX) scheme into not only NO_x emissions but also directly as ozone (Vinken et al., 2011). Clearly both the ship emissions and their immediate treatment is an important consideration, especially for near surface ozone and OH over remote maritime domains such as the Northern Pacific Ocean.

Underprediction of ozone and HO_x is a persistent problem in this northern domain and largely mirrors previously published studies involving the ARCTAS campaign, a field campaign that took place over the North American Arctic in April of 2008 (Jacob et al., 2010; Alvarado et al., 2010). For the same flights, we similarly find model underprediction of NO_x mixing ratios, especially above 2 km (Fig. S8). Underprediction of NO_x mixing ratios would explain some of the underprediction of ozone mixing ratios.

3.3.2 Aerosol uptake

As for the aerosol uptake of HO_2, the sensitivity of HO_2 mixing ratios to this factor has been noted before (Martin et al., 2003; Mao et al., 2010; Christian et al., 2017), but mostly in the Arctic where low NO_x mixing ratios and lower temperatures lead to longer HO_2 lifetimes. Indeed, we found greater sensitivity to this factor in the Anchorage based INTEX-B flights, the northernmost domain analyzed here. However, we also find similar sensitivities for HO_2 mixing ratios in different vertical bins for the other regions presented here. Like a similar study for a North American Arctic campaign (Christian et al., 2017), we also consistently find better agreement between HO_2 modeled and measured mixing ratios when aerosol uptake of HO_2 rates are reduced from its default rate of 0.20. In the case of the best 25 fitting ensemble member profiles, we find rates of anywhere between, 0.133 in Honolulu INTEX-B, 0.085 for Houston INTEX-B, 0.069 for INTEX-A, and 0.064 for Anchorage INTEX-B. For most of these cases, where we found greatest sensitivity to gamma HO_2, we also found HO_2 underprediction by GEOS-Chem. Thus, lower uptake rates alleviate some of this difference.

It is also possible that some of the underprediction of HO_2 by the model could be attributed to missing HO_2 sources or interferences in the measurements from peroxy radicals (Fuchs et al., 2011). As this interference requires the presence of alkenes or aromatics, it is more of a consideration near the surface and VOC emissions sources. While this is a consideration for the near surface HO_2 model underestimate in INTEX-A, it is not a major consideration for INTEX-B since much of that campaign took place over more remote maritime regions.

4 Conclusions

We have presented a global sensitivity analysis of GEOS-Chem modeled oxidants for the time period and flight tracks of the INTEX-NA field campaigns. Uncertainties and sensitivities of modeled ozone, OH, and HO_2 were found and shown in Figs. 6, 7, 8, and 9. In general, as evidenced by the small "missing" portion in the sensitivity graphs, we find model uncertainty to be overwhelmingly explained by uncertainties in individual factors with uncertainty arising from factor-factor interactions

typically less than 15 % of the total uncertainty. This suggests that uncertainties arisng from non-linear interactions between factors are generally small for the cases presented here. While there remains some disagreement between modeled and measured oxidant mixing ratios (Figs. 2, 3, 4, and 5), these differences were generally within the combined uncertainty ranges of both the modeled and measured values. In agreement with Travis et al. (2016), we find better model-measurement agreement for ozone with lower USA EPA-NEI emissions. With modeled ozone mixing ratios being most sensitive to lightning NO_x in the middle and upper troposphere, we find similarly better model-measurement agreement with lower lightning NO_x emissions for both INTEX-A and the INTEX-B Houston flights (Figs. 10 and 11). Recent work with parameterizing the nonlinear chemistry within lightning plumes in GEOS-Chem has found summertime Northern Hemispheric ozone and NO_x concentrations to decrease (Gressent et al., 2016) so it is possible that improving the parameterization of lightning NO_x may remedy some of this disagreement in future GEOS-Chem versions.

For some locations and altitudes, aerosol particle uptake of HO_2 can be responsible a large portion of uncertainty in HO_2 mixing ratios. In the case of the Anchorage based INTEX-B flights, gamma HO_2 was solely responsible for around half the uncertainty in HO_2 mixing ratios. While this sensitivity is not unexpected considering aerosol uptake of HO_2 has been shown to be important in poleward regions (Martin et al., 2003; Mao et al., 2010; Whalley et al., 2015; Christian et al., 2017), we also find considerable sensitivity to this factor in more southerly locations as well (Figs. 6, 7, 8, and 9). Similar to previous work for the ARCTAS campaign, we also find in all the regions presented here that lower uptake rates produce better model-measurement agreement (between 0.06 and 0.13 depending on the region as opposed to the default 0.20). With varied locations showing sensitivity to gamma HO_2, it appears that in order to model HO_2 with accuracy and certainty, aerosol uptake needs to be well accounted for and understood.

While the sensitivity results were different depending on the domain, the picture is similar from a distance. Emissions tended to be the dominant source of uncertainty for the modeled oxidants presented here, even for remote maritime domains. In all the cases, near surface ozone and OH are most sensitive to surface emissions sources, especially NO_x and, to a lesser extent, isoprene. We find similar sensitivities to lightning NO_x above 3 kilometers. For HO_2, carbon monoxide emissions, especially from biomass burning, and isoprene emissions are the dominant emissions uncertainty sources. Despite their considerably lower uncertainty, chemical factors such as kinetic rate coefficients, especially the NO_2 + OH reaction rate, and photolysis rates, such as those of ozone and NO_2 also were responsible for a considerable portion of the uncertainty. This is noteworthy considering uncertainties in these chemical factors tend to be much lower than those for emissions sources ($\sim$20-30 % vs. factors of 2-3 for emissions). This highlights the value in not only reducing emissions uncertainties, but also in making more laboratory measurements to provide more certainty for chemical factors, even those thought to be well known.

References

Alvarado, M. J., Logan, J. A., Mao, J., Apel, E., Riemer, D., Blake, D., Cohen, R. C., Min, K.-E., Perring, A. E., Browne, E. C., Wooldridge, P. J., Diskin, G. S., Sachse, G. W., Fuelberg, H., Sessions, W. R., Harrigan, D. L., Huey, G., Liao, J., Case-Hanks, A., Jimenez, J. L., Cubison, M. J., Vay, S. A., Weinheimer, A. J., Knapp, D. J., Montzka, D. D., Flocke, F. M., Pollack, I. B., Wennberg, P. O., Kurten, A., Crounse, J., Clair, J. M. S., Wisthaler, A., Mikoviny, T., Yantosca, R. M., Carouge, C. C., and Le Sager, P.: Nitrogen oxides and PAN in plumes from boreal fires during ARCTAS-B and their impact on ozone: an integrated analysis of aircraft and satellite observations, Atmos. Chem. Phys., 10, 9739–9760, doi:10.5194/acp-10-9739-2010, http://www.atmos-chem-phys.net/10/9739/2010/, 2010.

Bey, I., Jacob, D. J., Yantosca, R. M., Logan, J. A., Field, B. D., Fiore, A. M., Li, Q., Liu, H. Y., Mickley, L. J., and Schultz, M. G.: Global modeling of tropospheric chemistry with assimilated meteorology: Model description and evaluation, J. Geophys. Res., 106, 23 073–23 095, doi:10.1029/2001JD000807, http://onlinelibrary.wiley.com/doi/10.1029/2001JD000807/abstract, 2001.

Brewer, J. F., Bishop, M., Kelp, M., Keller, C. A., Ravishankara, A. R., and Fischer, E. V.: A sensitivity analysis of key natural factors in the modeled global acetone budget, J. Geophys. Res. Atmos., 122, 2016JD025 935, doi:10.1002/2016JD025935, http://onlinelibrary.wiley.com/doi/10.1002/2016JD025935/abstract, 2017.

Brune, W. H., Faloona, I. C., Tan, D., Weinheimer, A. J., Campos, T., Ridley, B. A., Vay, S. A., Collins, J. E., Sachse, G. W., Jaeglé, L., and Jacob, D. J.: Airborne in-situ OH and HO2 observations in the cloud-free troposphere and lower stratosphere during SUCCESS, Geophys. Res. Lett., 25, 1701–1704, doi:10.1029/97GL03098, http://onlinelibrary.wiley.com/doi/10.1029/97GL03098/abstract, 1998.

Chameides, W. and Walker, J. C. G.: A photochemical theory of tropospheric ozone, J. Geophys. Res., 78, 8751–8760, doi:10.1029/JC078i036p08751, http://onlinelibrary.wiley.com/doi/10.1029/JC078i036p08751/abstract, 1973.

Chen, S. and Brune, W. H.: Global sensitivity analysis of ozone production and O3–NOx–VOC limitation based on field data, Atmospheric Environment, 55, 288–296, doi:10.1016/j.atmosenv.2012.03.061, http://www.sciencedirect.com/science/article/pii/S1352231012003020, 2012.

Chen, S., Brune, W. H., Oluwole, O. O., Kolb, C. E., Bacon, F., Li, G., and Rabitz, H.: Global sensitivity analysis of the regional atmospheric chemical mechanism: an application of random sampling-high dimensional model representation to urban oxidation chemistry, Environ. Sci. Technol., 46, 11 162–11 170, doi:10.1021/es301565w, 2012.

Christian, K. E., Brune, W. H., and Mao, J.: Global sensitivity analysis of the GEOS-Chem chemical transport model: ozone and hydrogen oxides during ARCTAS (2008), Atmos. Chem. Phys., 17, 3769–3784, doi:10.5194/acp-17-3769-2017, http://www.atmos-chem-phys.net/17/3769/2017/, 2017.

Crawford, J., Davis, D., Olson, J., Chen, G., Liu, S., Gregory, G., Barrick, J., Sachse, G., Sandholm, S., Heikes, B., Singh, H., and Blake, D.: Assessment of upper tropospheric HOx sources over the tropical Pacific based on NASA GTE/PEM data: Net effect on HOx and other photochemical parameters, J. Geophys. Res., 104, 16 255–16 273, doi:10.1029/1999JD900106, http://onlinelibrary.wiley.com/doi/10.1029/1999JD900106/abstract, 1999.

de Gouw, J. A., Parrish, D. D., Frost, G. J., and Trainer, M.: Reduced emissions of CO2, NOx, and SO2 from U.S. power plants owing to switch from coal to natural gas with combined cycle technology, Earth's Future, 2, 75–82, doi:10.1002/2013EF000196, http://onlinelibrary.wiley.com/doi/10.1002/2013EF000196/abstract, 2014.

Fiore, A. M., Jacob, D. J., Bey, I., Yantosca, R. M., Field, B. D., Fusco, A. C., and Wilkinson, J. G.: Background ozone over the United States in summer: Origin, trend, and contribution to pollution episodes, J.-Geophys.-Res., 107, ACH 11–1, doi:10.1029/2001JD000982, http://onlinelibrary.wiley.com/doi/10.1029/2001JD000982/abstract, 2002.

Fiore, A. M., Horowitz, L. W., Purves, D. W., Levy, H., Evans, M. J., Wang, Y., Li, Q., and Yantosca, R. M.: Evaluating the contribution of changes in isoprene emissions to surface ozone trends over the eastern United States, J. Geophys. Res., 110, D12 303, doi:10.1029/2004JD005485, http://onlinelibrary.wiley.com/doi/10.1029/2004JD005485/abstract, 2005.

Fuchs, H., Bohn, B., Hofzumahaus, A., Holland, F., Lu, K. D., Nehr, S., Rohrer, F., and Wahner, A.: Detection of HO_2 by laser-induced fluorescence: calibration and interferences from RO_2 radicals, Atmospheric Measurement Techniques, 4, 1209–1225, doi:10.5194/amt-4-1209-2011, http://www.atmos-meas-tech.net/4/1209/2011/, 2011.

Gao, D., Stockwell, W. R., and Milford, J. B.: First-order sensitivity and uncertainty analysis for a regional-scale gas-phase chemical mechanism, J. Geophys. Res., 100, 23 153–23 166, doi:10.1029/95JD02704, http://onlinelibrary.wiley.com/doi/10.1029/95JD02704/abstract, 1995.

Gressent, A., Sauvage, B., Cariolle, D., Evans, M., Leriche, M., Mari, C., and Thouret, V.: Modeling lightning-NOx chemistry on a sub-grid scale in a global chemical transport model, Atmos. Chem. Phys., 16, 5867–5889, doi:10.5194/acp-16-5867-2016, http://www.atmos-chem-phys.net/16/5867/2016/, 2016.

Guenther, A. B., Jiang, X., Heald, C. L., Sakulyanontvittaya, T., Duhl, T., Emmons, L. K., and Wang, X.: The Model of Emissions of Gases and Aerosols from Nature version 2.1 (MEGAN2.1): an extended and updated framework for modeling biogenic emissions, Geosci. Model Dev., 5, 1471–1492, doi:10.5194/gmd-5-1471-2012, http://www.geosci-model-dev.net/5/1471/2012/, 2012.

Guerova, G., Bey, I., Attié, J.-L., Martin, R. V., Cui, J., and Sprenger, M.: Impact of transatlantic transport episodes on summertime ozone in Europe, Atmos. Chem. Phys., 6, 2057–2072, doi:10.5194/acp-6-2057-2006, http://www.atmos-chem-phys.net/6/2057/2006/, 2006.

Heald, C. L., Ridley, D. A., Kreidenweis, S. M., and Drury, E. E.: Satellite observations cap the atmospheric organic aerosol budget, Geophys. Res. Lett., 37, L24 808, doi:10.1029/2010GL045095, http://onlinelibrary.wiley.com/doi/10.1029/2010GL045095/abstract, 2010.

Henze, D. K., Hakami, A., and Seinfeld, J. H.: Development of the adjoint of GEOS-Chem, Atmos. Chem. Phys., 7, 2413–2433, doi:10.5194/acp-7-2413-2007, http://www.atmos-chem-phys.net/7/2413/2007/, 2007.

Hudman, R. C., Jacob, D. J., Turquety, S., Leibensperger, E. M., Murray, L. T., Wu, S., Gilliland, A. B., Avery, M., Bertram, T. H., Brune, W., Cohen, R. C., Dibb, J. E., Flocke, F. M., Fried, A., Holloway, J., Neuman, J. A., Orville, R., Perring, A., Ren, X., Sachse, G. W., Singh, H. B., Swanson, A., and Wooldridge, P. J.: Surface and lightning sources of nitrogen oxides over the United States: Magnitudes, chemical evolution, and outflow, J. Geophys. Res., 112, D12S05, doi:10.1029/2006JD007912, http://onlinelibrary.wiley.com/doi/10.1029/2006JD007912/abstract, 2007.

Huntrieser, H., Schlager, H., Roiger, A., Lichtenstern, M., Schumann, U., Kurz, C., Brunner, D., Schwierz, C., Richter, A., and Stohl, A.: Lightning-produced NOx over Brazil during TROCCINOX: airborne measurements in tropical and subtropical thunderstorms and the importance of mesoscale convective systems, Atmos. Chem. Phys., 7, 2987–3013, doi:10.5194/acp-7-2987-2007, http://www.atmos-chem-phys.net/7/2987/2007/, 2007.

Huntrieser, H., Schumann, U., Schlager, H., Höller, H., Giez, A., Betz, H.-D., Brunner, D., Forster, C., Pinto Jr., O., and Calheiros, R.: Lightning activity in Brazilian thunderstorms during TROCCINOX: implications for NOx production, Atmos. Chem. Phys., 8, 921–953, doi:10.5194/acp-8-921-2008, http://www.atmos-chem-phys.net/8/921/2008/, 2008.

Jacob, D. J.: Heterogeneous chemistry and tropospheric ozone, Atmospheric Environment, 34, 2131–2159, doi:10.1016/S1352-2310(99)00462-8, http://www.sciencedirect.com/science/article/pii/S1352231099004628, 2000.

Jacob, D. J., Crawford, J. H., Maring, H., Clarke, A. D., Dibb, J. E., Emmons, L. K., Ferrare, R. A., Hostetler, C. A., Russell, P. B., Singh, H. B., Thompson, A. M., Shaw, G. E., McCauley, E., Pederson, J. R., and Fisher, J. A.: The Arctic Research of the Composition of the

Troposphere from Aircraft and Satellites (ARCTAS) mission: design, execution, and first results, Atmos. Chem. Phys., 10, 5191–5212, doi:10.5194/acp-10-5191-2010, http://www.atmos-chem-phys.net/10/5191/2010/, 2010.

Jaeglé, L., Steinberger, L., Martin, R. V., and Chance, K.: Global partitioning of NOx sources using satellite observations: Relative roles of fossil fuel combustion, biomass burning and soil emissions, Faraday Discussions, 130, 407, doi:10.1039/b502128f, http://xlink.rsc.org/?DOI=b502128f, 2005.

Kalos, M. H. and Whitlock, P. A.: Monte Carlo Methods: Basics, J. Wiley & Sons, 1986.

Li, G., Rosenthal, C., and Rabitz, H.: High Dimensional Model Representations, J. Phys. Chem. A, 105, 7765–7777, doi:10.1021/jp010450t, http://dx.doi.org/10.1021/jp010450t, 2001.

Li, G., Wang, S.-W., and Rabitz, H.: Practical Approaches To Construct RS-HDMR Component Functions, The Journal of Physical Chemistry A, 106, 8721–8733, doi:10.1021/jp014567t, http://dx.doi.org/10.1021/jp014567t, 2002.

Li, G., Rabitz, H., Wang, S.-W., and Georgopoulos, P. G.: Correlation method for variance reduction of Monte Carlo integration in RS-HDMR, J. Comput. Chem., 24, 277–283, doi:10.1002/jcc.10172, http://onlinelibrary.wiley.com/doi/10.1002/jcc.10172/abstract, 2003.

Li, G., Rabitz, H., Yelvington, P. E., Oluwole, O. O., Bacon, F., Kolb, C. E., and Schoendorf, J.: Global Sensitivity Analysis for Systems with Independent and/or Correlated Inputs, J. Phys. Chem. A, 114, 6022–6032, doi:10.1021/jp9096919, http://dx.doi.org/10.1021/jp9096919, 2010.

Liaskos, C. E., Allen, D. J., and Pickering, K. E.: Sensitivity of tropical tropospheric composition to lightning NOx production as determined by replay simulations with GEOS-5, J. Geophys. Res. Atmos., 120, 2014JD022 987, doi:10.1002/2014JD022987, http://onlinelibrary.wiley.com/doi/10.1002/2014JD022987/abstract, 2015.

Lin, M., Horowitz, L. W., Payton, R., Fiore, A. M., and Tonnesen, G.: US surface ozone trends and extremes from 1980 to 2014: quantifying the roles of rising Asian emissions, domestic controls, wildfires, and climate, Atmos. Chem. Phys., 17, 2943–2970, doi:10.5194/acp-17-2943-2017, http://www.atmos-chem-phys.net/17/2943/2017/, 2017.

Lu, X., Wang, Y.-P., Ziehn, T., and Dai, Y.: An efficient method for global parameter sensitivity analysis and its applications to the Australian community land surface model (CABLE), Agricultural and Forest Meteorology, 182–183, 292–303, doi:10.1016/j.agrformet.2013.04.003, http://www.sciencedirect.com/science/article/pii/S0168192313000804, 2013.

Mao, J., Jacob, D. J., Evans, M. J., Olson, J. R., Ren, X., Brune, W. H., Clair, J. M. S., Crounse, J. D., Spencer, K. M., Beaver, M. R., Wennberg, P. O., Cubison, M. J., Jimenez, J. L., Fried, A., Weibring, P., Walega, J. G., Hall, S. R., Weinheimer, A. J., Cohen, R. C., Chen, G., Crawford, J. H., McNaughton, C., Clarke, A. D., Jaeglé, L., Fisher, J. A., Yantosca, R. M., Le Sager, P., and Carouge, C.: Chemistry of hydrogen oxide radicals (HOx) in the Arctic troposphere in spring, Atmos. Chem. Phys., 10, 5823–5838, doi:10.5194/acp-10-5823-2010, http://www.atmos-chem-phys.net/10/5823/2010/, 2010.

Mao, J., Ren, X., Zhang, L., Van Duin, D. M., Cohen, R. C., Park, J.-H., Goldstein, A. H., Paulot, F., Beaver, M. R., Crounse, J. D., Wennberg, P. O., DiGangi, J. P., Henry, S. B., Keutsch, F. N., Park, C., Schade, G. W., Wolfe, G. M., Thornton, J. A., and Brune, W. H.: Insights into hydroxyl measurements and atmospheric oxidation in a California forest, Atmos. Chem. Phys., 12, 8009–8020, doi:10.5194/acp-12-8009-2012, http://www.atmos-chem-phys.net/12/8009/2012/, 2012.

Mao, J., Fan, S., Jacob, D. J., and Travis, K. R.: Radical loss in the atmosphere from Cu-Fe redox coupling in aerosols, Atmos. Chem. Phys., 13, 509–519, doi:10.5194/acp-13-509-2013, http://www.atmos-chem-phys.net/13/509/2013/, 2013a.

Mao, J., Paulot, F., Jacob, D. J., Cohen, R. C., Crounse, J. D., Wennberg, P. O., Keller, C. A., Hudman, R. C., Barkley, M. P., and Horowitz, L. W.: Ozone and organic nitrates over the eastern United States: Sensitivity to isoprene chemistry, J. Geophys. Res. Atmos., 118, 2013JD020 231, doi:10.1002/jgrd.50817, http://onlinelibrary.wiley.com/doi/10.1002/jgrd.50817/abstract, 2013b.

Martin, R. V., Jacob, D. J., Yantosca, R. M., Chin, M., and Ginoux, P.: Global and regional decreases in tropospheric oxidants from photochemical effects of aerosols, J. Geophys. Res., 108, 4097, doi:10.1029/2002JD002622, http://onlinelibrary.wiley.com/doi/10.1029/2002JD002622/abstract, 2003.

McLinden, C. A., Olsen, S. C., Hannegan, B., Wild, O., Prather, M. J., and Sundet, J.: Stratospheric ozone in 3-D models: A simple chemistry and the cross-tropopause flux, J. Geophys. Res., 105, 14 653–14 665, doi:10.1029/2000JD900124, http://onlinelibrary.wiley.com/doi/10.1029/2000JD900124/abstract, 2000.

Morris, M. D.: Factorial Sampling Plans for Preliminary Computational Experiments, Technometrics, 33, 161–174, doi:10.1080/00401706.1991.10484804, http://www.tandfonline.com/doi/abs/10.1080/00401706.1991.10484804, 1991.

Newsome, B. and Evans, M.: Impact of uncertainties in inorganic chemical rate constants on tropospheric composition and ozone radiative forcing, Atmos. Chem. Phys. Discuss., 2017, 1–28, doi:10.5194/acp-2017-12, http://www.atmos-chem-phys-discuss.net/acp-2017-12/, 2017.

Olson, J. R., Crawford, J. H., Chen, G., Fried, A., Evans, M. J., Jordan, C. E., Sandholm, S. T., Davis, D. D., Anderson, B. E., Avery, M. A., Barrick, J. D., Blake, D. R., Brune, W. H., Eisele, F. L., Flocke, F., Harder, H., Jacob, D. J., Kondo, Y., Lefer, B. L., Martinez, M., Mauldin, R. L., Sachse, G. W., Shetter, R. E., Singh, H. B., Talbot, R. W., and Tan, D.: Testing fast photochemical theory during TRACE-P based on measurements of OH, HO2, and CH2O, J. Geophys. Res., 109, D15S10, doi:10.1029/2003JD004278, http://onlinelibrary.wiley.com/doi/10.1029/2003JD004278/abstract, 2004.

Ott, L. E., Bacmeister, J., Pawson, S., Pickering, K., Stenchikov, G., Suarez, M., Huntrieser, H., Loewenstein, M., Lopez, J., and Xueref-Remy, I.: Analysis of Convective Transport and Parameter Sensitivity in a Single Column Version of the Goddard Earth Observation System, Version 5, General Circulation Model, J. Atmos. Sci., 66, 627–646, doi:10.1175/2008JAS2694.1, http://journals.ametsoc.org/doi/abs/10.1175/2008JAS2694.1, 2009.

Price, C. and Rind, D.: A simple lightning parameterization for calculating global lightning distributions, J. Geophys. Res., 97, 9919–9933, doi:10.1029/92JD00719, http://onlinelibrary.wiley.com/doi/10.1029/92JD00719/abstract, 1992.

Qu, Z., Henze, D. K., Capps, S. L., Wang, Y., Xu, X., Wang, J., and Keller, M.: Monthly top-down NOx emissions for China (2005–2012): A hybrid inversion method and trend analysis, J. Geophys. Res. Atmos., p. 2016JD025852, doi:10.1002/2016JD025852, http://onlinelibrary.wiley.com/doi/10.1002/2016JD025852/abstract, 2017.

Rabitz, H. and Aliş, O. F.: General foundations of high-dimensional model representations, Journal of Mathematical Chemistry, 25, 197–233, doi:10.1023/A:1019188517934, http://link.springer.com/article/10.1023/A:1019188517934, 1999.

Ren, X., Harder, H., Martinez, M., Faloona, I. C., Tan, D., Lesher, R. L., Carlo, P. D., Simpas, J. B., and Brune, W. H.: Interference Testing for Atmospheric HOx Measurements by Laser-induced Fluorescence, Journal of Atmospheric Chemistry, 47, 169–190, doi:10.1023/B:JOCH.0000021037.46866.81, https://link.springer.com/article/10.1023/B:JOCH.0000021037.46866.81, 2004.

Ren, X., Olson, J. R., Crawford, J. H., Brune, W. H., Mao, J., Long, R. B., Chen, Z., Chen, G., Avery, M. A., Sachse, G. W., Barrick, J. D., Diskin, G. S., Huey, L. G., Fried, A., Cohen, R. C., Heikes, B., Wennberg, P. O., Singh, H. B., Blake, D. R., and Shetter, R. E.: HOx chemistry during INTEX-A 2004: Observation, model calculation, and comparison with previous studies, J. Geophys. Res., 113, D05 310, doi:10.1029/2007JD009166, http://onlinelibrary.wiley.com/doi/10.1029/2007JD009166/abstract, 2008.

Saltelli, A., Ratto, M., Andres, T., Campolongo, F., Cariboni, J., Gatelli, D., Saisana, M., and Tarantola, S.: Global Sensitivity Analysis: The Primer, John Wiley & Sons, 2008.

Sander, S., Abbatt, J., Barker, J., Burkholder, J., Friedl, R., Golden, D., Huie, R., Kolb, C., Kurylo, M., Moortgat, G., Orkin, V., and Wine, P.: Chemical Kinetics and Photochemical Data for Use in Atmospheric Studies Evaluation Number 17, JPL Publication 10-6, 2011.

Schumann, U. and Huntrieser, H.: The global lightning-induced nitrogen oxides source, Atmos. Chem. Phys., 7, 3823–3907, doi:10.5194/acp-7-3823-2007, http://www.atmos-chem-phys.net/7/3823/2007/, 2007.

Singh, H. B., Brune, W. H., Crawford, J. H., Jacob, D. J., and Russell, P. B.: Overview of the summer 2004 Intercontinental Chemical Transport Experiment–North America (INTEX-A), J. Geophys. Res., 111, D24S01, doi:10.1029/2006JD007905, http://onlinelibrary.wiley.com/doi/10.1029/2006JD007905/abstract, 2006.

Singh, H. B., Brune, W. H., Crawford, J. H., Flocke, F., and Jacob, D. J.: Chemistry and transport of pollution over the Gulf of Mexico and the Pacific: spring 2006 INTEX-B campaign overview and first results, Atmos. Chem. Phys., 9, 2301–2318, doi:10.5194/acp-9-2301-2009, http://www.atmos-chem-phys.net/9/2301/2009/, 2009.

Sobol, I. M.: Uniformly distributed sequences with an additional uniform property, USSR Computational Mathematics and Mathematical Physics, 16, 236–242, doi:10.1016/0041-5553(76)90154-3, http://www.sciencedirect.com/science/article/pii/0041555376901543, 1976.

Travis, K. R., Jacob, D. J., Fisher, J. A., Kim, P. S., Marais, E. A., Zhu, L., Yu, K., Miller, C. C., Yantosca, R. M., Sulprizio, M. P., Thompson, A. M., Wennberg, P. O., Crounse, J. D., St. Clair, J. M., Cohen, R. C., Laughner, J. L., Dibb, J. E., Hall, S. R., Ullmann, K., Wolfe, G. M., Pollack, I. B., Peischl, J., Neuman, J. A., and Zhou, X.: Why do models overestimate surface ozone in the Southeast United States?, Atmos. Chem. Phys., 16, 13 561–13 577, doi:10.5194/acp-16-13561-2016, http://www.atmos-chem-phys.net/16/13561/2016/, 2016.

Verstraeten, W. W., Neu, J. L., Williams, J. E., Bowman, K. W., Worden, J. R., and Boersma, K. F.: Rapid increases in tropospheric ozone production and export from China, Nature Geosci, 8, 690–695, doi:10.1038/ngeo2493, http://www.nature.com/ngeo/journal/v8/n9/abs/ngeo2493.html, 2015.

Vinken, G. C. M., Boersma, K. F., Jacob, D. J., and Meijer, E. W.: Accounting for non-linear chemistry of ship plumes in the GEOS-Chem global chemistry transport model, Atmos. Chem. Phys., 11, 11 707–11 722, doi:10.5194/acp-11-11707-2011, http://www.atmos-chem-phys.net/11/11707/2011/, 2011.

Vinken, G. C. M., Boersma, K. F., Maasakkers, J. D., Adon, M., and Martin, R. V.: Worldwide biogenic soil NOx emissions inferred from OMI NO2 observations, Atmos. Chem. Phys., 14, 10 363–10 381, doi:10.5194/acp-14-10363-2014, http://www.atmos-chem-phys.net/14/10363/2014/, 2014.

Weinheimer, A. J., Walega, J. G., Ridley, B. A., Gary, B. L., Blake, D. R., Blake, N. J., Rowland, F. S., Sachse, G. W., Anderson, B. E., and Collins, J. E.: Meridional distributions of NOx, NOy, and other species in the lower stratosphere and upper troposphere during AASE II, Geophys. Res. Lett., 21, 2583–2586, doi:10.1029/94GL01897, http://onlinelibrary.wiley.com/doi/10.1029/94GL01897/abstract, 1994.

Whalley, L. K., Stone, D., George, I. J., Mertes, S., van Pinxteren, D., Tilgner, A., Herrmann, H., Evans, M. J., and Heard, D. E.: The influence of clouds on radical concentrations: observations and modelling studies of HOx during the Hill Cap Cloud Thuringia (HCCT) campaign in 2010, Atmos. Chem. Phys., 15, 3289–3301, doi:10.5194/acp-15-3289-2015, http://www.atmos-chem-phys.net/15/3289/2015/, 2015.

Wild, O. and Prather, M. J.: Global tropospheric ozone modeling: Quantifying errors due to grid resolution, J. Geophys. Res., 111, D11 305, doi:10.1029/2005JD006605, http://onlinelibrary.wiley.com/doi/10.1029/2005JD006605/abstract, 2006.

Wu, S., Mickley, L. J., Jacob, D. J., Logan, J. A., Yantosca, R. M., and Rind, D.: Why are there large differences between models in global budgets of tropospheric ozone?, J. Geophys. Res., 112, D05 302, doi:10.1029/2006JD007801, http://onlinelibrary.wiley.com/doi/10.1029/2006JD007801/abstract, 2007.

Xu, X., Wang, J., Henze, D. K., Qu, W., and Kopacz, M.: Constraints on aerosol sources using GEOS-Chem adjoint and MODIS radiances, and evaluation with multisensor (OMI, MISR) data, Journal of Geophysical Research: Atmospheres, 118, 6396–6413, doi:10.1002/jgrd.50515, http://dx.doi.org/10.1002/jgrd.50515, 2013.

Yang, Y.-J., Stockwell, W. R., and Milford, J. B.: Uncertainties in Incremental Reactivities of Volatile Organic Compounds, Environ. Sci. Technol., 29, 1336–1345, doi:10.1021/es00005a028, http://dx.doi.org/10.1021/es00005a028, 1995.

Zhang, L., Jacob, D. J., Yue, X., Downey, N. V., Wood, D. A., and Blewitt, D.: Sources contributing to background surface ozone in the US Intermountain West, Atmos. Chem. Phys., 14, 5295–5309, doi:10.5194/acp-14-5295-2014, http://www.atmos-chem-phys.net/14/5295/2014/, 2014.

Ziehn, T. and Tomlin, A. S.: GUI–HDMR – A software tool for global sensitivity analysis of complex models, Environmental Modelling & Software, 24, 775–785, doi:10.1016/j.envsoft.2008.12.002, http://www.sciencedirect.com/science/article/pii/S1364815208002168, 2009.

Ziehn, T., Hughes, K. J., Griffiths, J. F., Porter, R., and Tomlin, A. S.: A global sensitivity study of cyclohexane oxidation under low temperature fuel-rich conditions using HDMR methods, Combustion Theory and Modelling, 13, 589–605, doi:10.1080/13647830902878398, http://www.tandfonline.com/doi/abs/10.1080/13647830902878398, 2009.

Table 1. Factors included in INTEX-A RS-HDMR analysis and their respective uncertainties. OC is organic carbon, MP is methylhydroperoxide, and MO_2 is methylperoxy radical. Uncertainties are expressed as multiplicative factors, except as noted in meteorological factors.

Factor	Uncertainty[#]	Factor	Uncertainty[#]
Emissions		**Photolysis**	
Biomass CO, NO_x, OC		j [$BrNO_3$]	1.4[d]
Soil NO_x	3.0[a]	j [CH_2O]	1.4[d]
Methyl Bromoform ($CHBr_3$)		j [H_2O_2]	1.3[d]
EPA (USA) CO, NH_3, NO_x		j [HNO_3]	1.3[d]
Streets (E. Asian) CO, NH_3, NO_x, SO_2	2.0	j [HOBr]	2.0[d]
Ship NO_x		j [NO_2]	1.2[d]
Isoprene	2.0[b]	j [O_3]	1.2[d]
Lightning NO_x	2.0[c]	**Meteorology**	
Kinetics		Cloud mass flux	1.5[f]
k [HNO_2] [OH]	1.5[d]	Relative humidity	5 %[g]
k [HNO_3] [OH]	1.2[d]	Soil Wetness	8.8 %[e]
k [HO_2] [HO_2]	1.15 / 1.2[*d]	Specific Humidity	5 %[g]
k [HO_2] [NO]	1.15[d]	Temperature	1.8 K[e]
k [MO_2] [HO_2]	1.3[d]	**Heterogeneous**	
k [MO_2] [NO]	1.15[d]	Gamma HO_2	3.0[d]
k [NO_2] [OH]	1.3[d]		
k [O_3] [HO_2]	1.15[d]		
k [O_3] [NO]	1.1[d]		
k [OH] [CH_4]	1.1[d]		
k [OH] [HO_2]	1.15[d]		

[#] at 1σ uncertainty confidence; [*] high pressure limit / low pressure limit uncertainties; [a] Jaeglé et al. (2005); [b] Guenther et al. (2012); [c] Liaskos et al. (2015); [d] Sander et al. (2011); [e] GEOS5-GEOS4; [f] Ott et al. (2009); [g] Heald et al. (2010)

Table 2. Factors included in INTEX-B RS-HDMR analysis and their respective uncertainties. OC is organic carbon, MP is methylhydroper-oxide, and MO_2 is methylperoxy radical. Uncertainties are expressed as multiplicative factors, except as noted in meteorological factors.

Factor	Uncertainty[#]	Factor	Uncertainty[#]
Emissions		**Photolysis**	
Biomass CO, NH_3, NO_x, OC	3.0[a]	j [CH_2O]	1.4[d]
Soil NO_x		j [H_2O_2]	1.3[d]
Methyl Bromoform ($CHBr_3$)		j [HNO_3]	1.3[d]
EDGAR NO_x		j [HOBr]	2.0[d]
EMEP (European) NO_x		j [MP]	1.5[d]
EPA (USA) CO, NO_x	2.0	j [NO_2]	1.2[d]
Streets (E. Asian) CO, NH_3, NO_x, SO_2		j [O_3]	1.2[d]
Ship NO_x		**Meteorology**	
Strat-Trop Exchange O_3		Cloud fraction	8.5 %[e]
Isoprene	2.0[b]	Cloud mass flux	1.5[f]
Lightning NO_x	2.0[c]	Relative Humidity	5 %[g]
Kinetics		Soil Wetness	8.8 %[e]
k [HNO_3] [OH]	1.2[d]	Specific Humidity	5 %[g]
k [HO_2] [HO_2]	1.15 / 1.2[*d]	Temperature	1.8 K[e]
k [HO_2] [NO]	1.15[d]	U Wind	0.71 ms^{-1e}
k [MO_2] [HO_2]	1.3[d]	**Heterogeneous**	
k [MO_2] [NO]	1.15[d]	Gamma HO_2	3.0[d]
k [MP] [OH]	1.4[d]	Gamma NO_2	3.0[d]
k [NO_2] [OH]	1.3[d]	Henry's Law HOBr	10.0[d]
k [O_3] [HO_2]	1.15[d]		
k [O_3] [NO]	1.1[d]		
k [O_3] [NO_2]	1.15[d]		
k [OH] [CH_4]	1.1[d]		
k [OH] [HO_2]	1.15[d]		

at 1σ uncertainty confidence; * high pressure limit / low pressure limit uncertainties; [a] Jaeglé et al. (2005); [b] Guenther et al. (2012); [c] Liaskos et al. (2015); [d] Sander et al. (2011); [e] GEOS5-GEOS4; [f] Ott et al. (2009); [g] Heald et al. (2010)
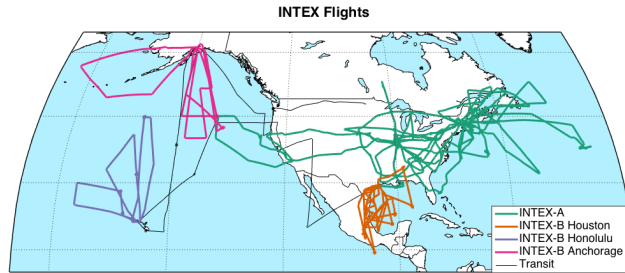
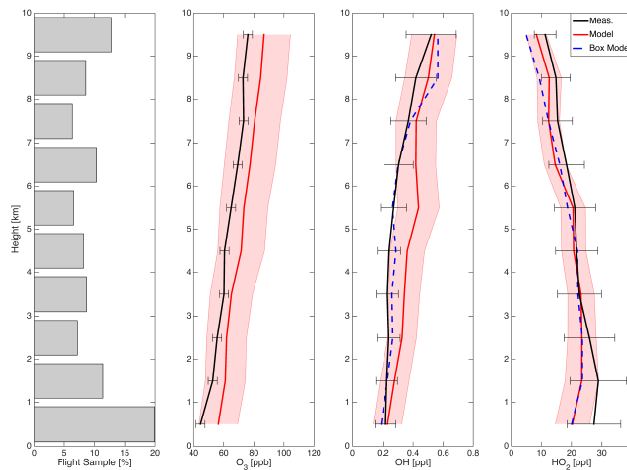**Figure 1.** Map of INTEX-A & INTEX-B flights

Figure 2. Vertical profiles of median modeled (red) and measured (black) ozone, OH, and HO$_2$ for INTEX-A flight data binned by kilometer. Gray bar graph shows percent of flight data within each vertical bin. Shaded regions represent 1σ of model ensemble; error bars on measurements are uncertainty at 1σ confidence. Blue line represents results from box model (Ren et al., 2008).
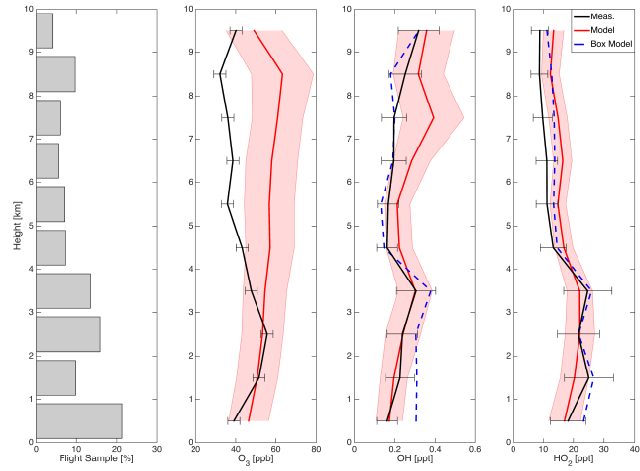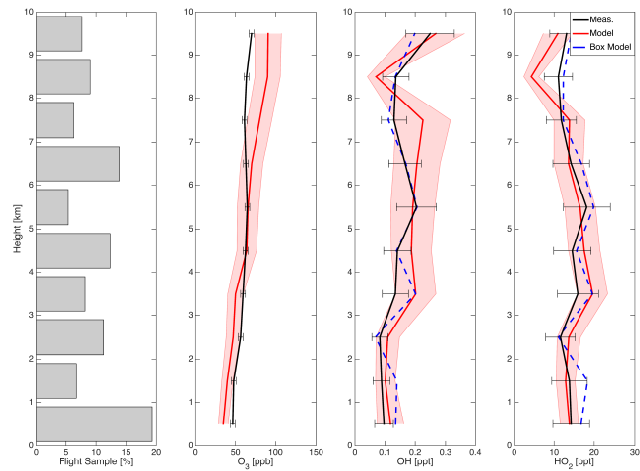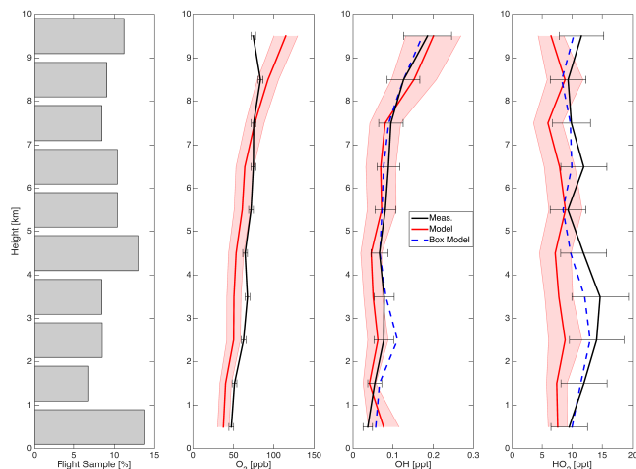
Figure 3. Vertical profiles of median modeled (red) and measured (black) ozone, OH, and HO$_2$ for Houston based INTEX-B flight data binned by kilometer. Gray bar graph shows percent of flight data within each vertical bin. Shaded regions represent 1σ of model ensemble; error bars on measurements are uncertainty at 1σ confidence. Blue line represents results from box model


Figure 4. Vertical profiles of median modeled (red) and measured (black) ozone, OH, and HO$_2$ for Honolulu based INTEX-B flight data binned by kilometer. Gray bar graph shows percent of flight data within each vertical bin. Shaded regions represent 1σ of model ensemble; error bars on measurements are uncertainty at 1σ confidence. Blue line represents results from box model

Figure 5. Vertical profiles of median modeled (red) and measured (black) ozone, OH, and HO_2 for Anchorage based INTEX-B flight data binned by kilometer. Gray bar graph shows percent of flight data within each vertical bin. Shaded regions represent 1σ of model ensemble; error bars on measurements are uncertainty at 1σ confidence. Blue line represents results from box model
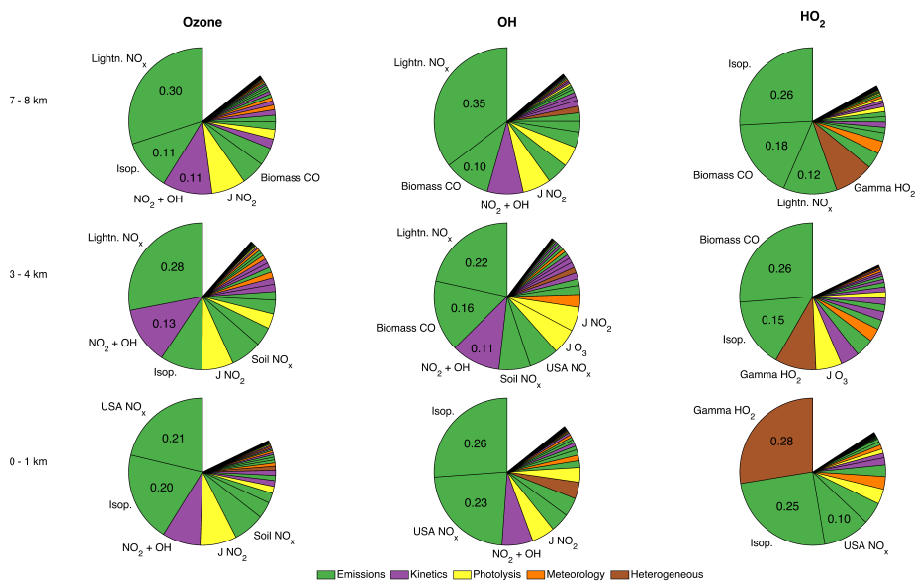
Figure 6. First order sensitivity indices for median flight track ozone, OH, and HO_2 for INTEX-A flights. Legend categories are defined in Table 1. Sensitivity indices are labeled in pie slices for factors for which $S_i \geq 0.10$
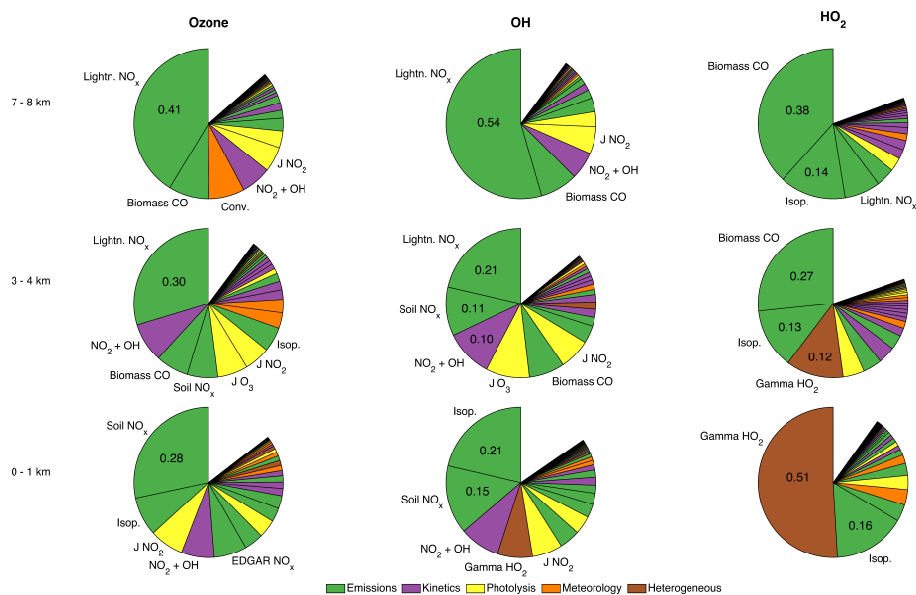
Figure 7. First order sensitivity indices for median flight track ozone, OH, and HO$_2$ for INTEX-B flights originating from and terminating in Houston. Legend categories are defined in Table 2. Sensitivity indices are labeled in pie slices for factors for which S$_i \geq 0.10$
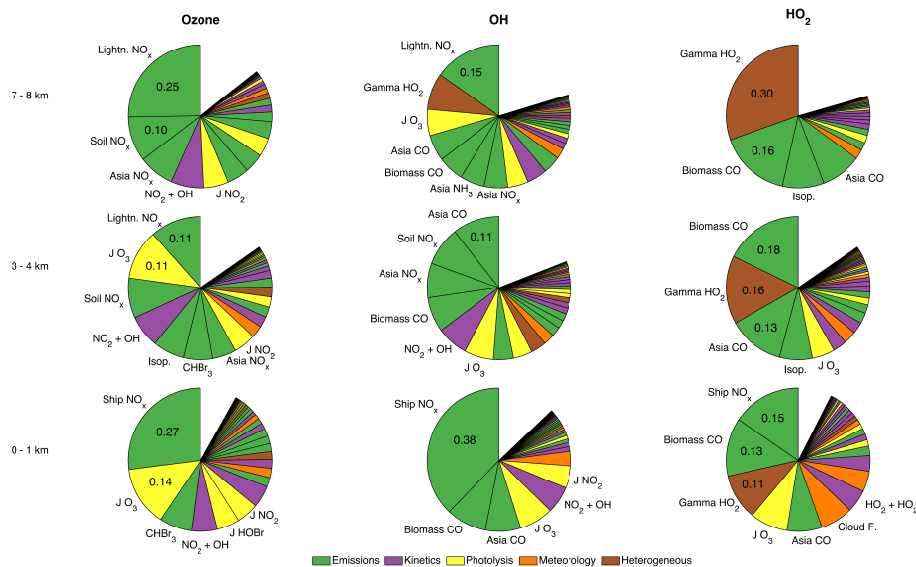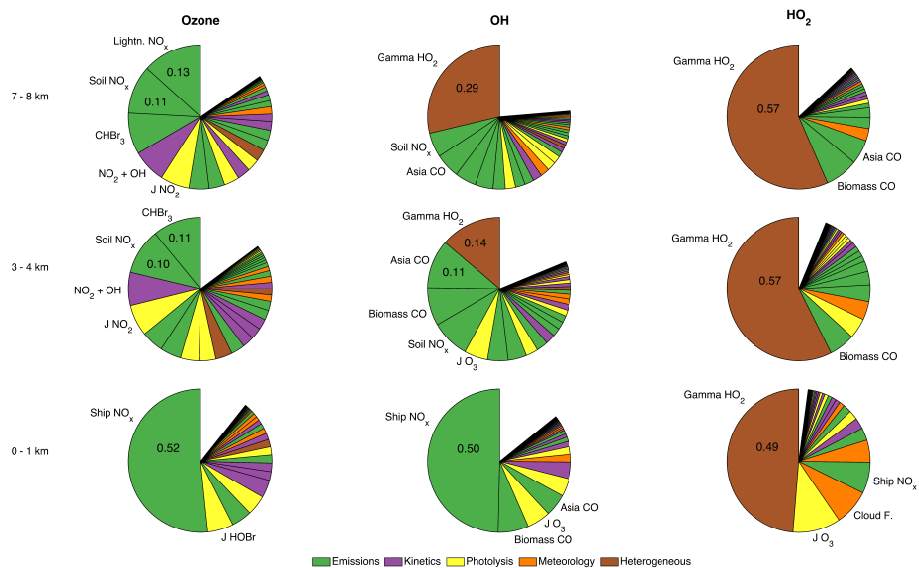

Figure 8. First order sensitivity indices for median flight track ozone, OH, and HO$_2$ for INTEX-B flights originating from and terminating in Honolulu. Legend categories are defined in Table 2. Sensitivity indices are labeled in pie slices for factors for which S$_i \geq 0.10$

Figure 9. First order sensitivity indices for median flight track ozone, OH, and HO$_2$ for INTEX-B flights originating from and terminating in Anchorage. Legend categories are defined in Table 2. Sensitivity indices are labeled in pie slices for factors for which S$_i \geq 0.10$
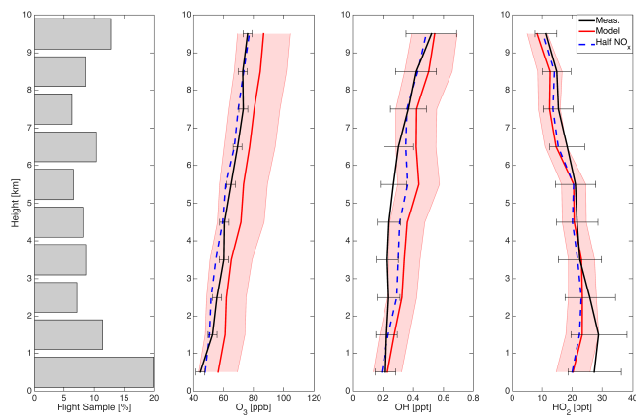

Figure 10. Vertical profiles of median modeled (red) and measured (black) ozone, OH, and HO$_2$ INTEX-A flight data binned by kilometer. Gray bar graph shows percent of flight data within each vertical bin. Shaded regions represent 1σ of model ensemble; error bars on measurements are uncertainty at 1σ confidence. Blue line represents EPA-NEI and lightning NO$_x$ emissions reduced by 50 %
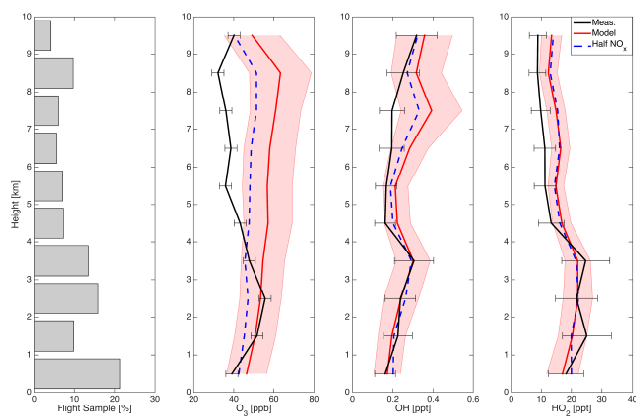
Figure 11. Vertical profiles of median modeled (red) and measured (black) ozone, OH, and HO$_2$ Houston based INTEX-B flight data binned by kilometer. Gray bar graph shows percent of flight data within each vertical bin. Shaded regions represent 1σ of model ensemble; error bars on measurements are uncertainty at 1σ confidence. Blue line represents EPA-NEI and lightning NO$_x$ emissions reduced by 50 %